

A small cytotoxic peptide from frog elicits potent antitumor immunity to prevent local tumor growth and metastases

Xue Qiao¹, Huixin Yang¹, Jiuxiang Gao¹, Shasha Cai¹, Nannan Shi¹, Mengke Wang¹, Yipeng Wang^{*,2} & Haining Yu^{*,1}

¹School of bioengineering, Dalian University of Technology, Dalian, Liaoning 116024, China

²Department of Pharmaceutical Sciences, College of Pharmaceutical Sciences, Soochow University, Suzhou, Jiangsu 215123, China

*Author for correspondence: Tel./Fax: +86 411 847 08850; yuhaining@dlut.edu.cn

**Author for correspondence: Tel./Fax: +86 512 658 82090; yipengwang@suda.edu.cn

Aim: Anticancer immunochemotherapy represents an attractive paradigm to improve therapeutic responses and reduce side effects. **Results & methodology:** Here, we show that a naturally occurring host defense peptide, HN-1 inhibited multiple malignant cells proliferation and tumor growth in a xenografted human breast tumor model. Acting through MAPK/NF-κB pathways, HN-1 induced a caspase-independent mitochondrial apoptosis, as indicated by a p53-dependent increase of Bax/Bcl-2 ratio and the nuclear translocation of apoptosis inducing factor. Besides, HN-1 augmented CD4⁺/CD8⁺ T cells in 4T1 mammary carcinoma model, by enhancing the serum levels of cancer immunity-associated effectors. Meanwhile, HN-1 decreased the angiogenesis and infiltration of the tumor-associated macrophages. **Conclusion:** HN-1 induces caspase-independent cancer cells apoptosis and boosts cancer-resolving immunity without inducing potentially harmful pro-inflammatory responses.

First draft submitted: 3 April 2019; Accepted for publication: 28 June 2019; Published online: 21 October 2019

Keywords: anticancer immunity • biodistribution • caspase-independent apoptosis • host defense peptides (HDPs) • immune-based mechanism

Chemotherapy is one of the mainstay medical disciplines specifically devoted to cure cancer [1]. Conventional chemotherapeutic agents are cytotoxic by interfering with cell division and inducing apoptosis [2]. Thereby, they usually associated with significant and cumulative systematic toxicities [3,4], and more likelihood that cancer cells become chemoresistant [5,6]. Herein, lately the immunostimulatory agents including cytokines and antibodies, especially the antibodies named ‘checkpoint inhibitors’, have been garnering significant attention for their impressive antitumor therapeutics. They directly enhance the function of T cells by either blocking the negative regulators of T-cell immunity of cytotoxic T-lymphocyte antigen 4 (CTLA-4) and programed death receptor-1 (PD-1) [7,8], or enhancing the costimulatory molecules, such as glucocorticoid-induced TNF receptor (GITR), OX40 and 4-1BB [8,9]. However, serious toxicities induced by systemic administration, including approved IL-2 and IFN-α, hinder dosing and their efficacy [10,11]. Besides, checkpoint-blocking antibodies are not encouraged on patients’ response patterns in a couple of aspects: induction of an apparent transient worsening of disease; a relatively much longer onset time in contrast to chemotherapy; and significant individual differences in patient response [7,12,13].

Further, great interest has been drawn to develop combinatorial immunotherapeutic interventions by combining chemo- or radiotherapeutic regimens with immunotherapy [14,15]. Thus, an ever increasing amount of literatures have borne out a strong immunological rationale that combining distinct mechanisms of chemotherapeutic and immune-modulatory can synergistically enhance the antitumor therapies [16,17]. Some chemotherapeutics are known to directly exert immunostimulatory effects and elicit an immune response both innately and adaptively [18,19]. However, the effectiveness of chemotherapy-elicited immune response is limited by various negative feedback mechanisms rising in tumor development during treatment [20,21]. Other strategy of combining chemo- and immunotherapeutic agent was consistently hampered by the lack of a management to effectively co-deliver them

to the tumors due to different physical and pharmacokinetic profiles [22], in addition to the much increased costs that present major challenges in the preclinical evaluations.

Host defense peptides (HDPs) are a group of evolutionarily conserved innate immune factors. They are widely distributed in nearly all kinds of animals and broadly participate in boosting and modulating host immune responses [23,24]. So far, many HDPs including well-studied melittin, cecropin B, magainins, BMAP-28, human cathelicidin-LL37 and lactoferrin, have been reported to have potent antitumor effect both *in vitro* and *in vivo* [25–27]. Growing evidences suggest that some natural HDPs trigger a range of immunomodulatory responses [28,29], among which of particular interest is their modulating the activation and differentiation of macrophages, T lymphocytes, and dendritic cells and to effectively restrain tumor cell proliferation and dissemination [30]. However, development of natural HDPs has been problematic owing to their detrimental activities, such as the induction of toxicities, including mast cell degranulation and apoptosis [31]. HN-1 is a naturally occurring HDP identified from Hainan cascade frog, *Amolops hainanensis*. In the present study, we showed that HN-1 possess potent *in vitro* and *in vivo* antitumor function with special mechanism. HN-1 triggers immunomodulatory responses and decreased the angiogenesis and infiltration of the tumor-associated macrophages (TAMs). Meanwhile, HN-1 exhibited good safety and ideal *in vivo* biodistribution. Overall, HN-1 represents a novel immunochemotherapeutic agent with improved efficacy and safety, and may shed light on the design of rationale-based combined cancer treatment.

Experimental sections

Peptide, cells & reagents

HN-1 was synthesized by Fmoc chemistry-based solid-phase synthesis on an automated peptide synthesizer. The purity (>95%) and identity of synthetic peptide was then confirmed by high-performance liquid chromatography (HPLC, Agela Technologies, Tianjin, China) and electronic spray ionization–mass spectrometry (ESI–MS, Shimadzu, Kyoto, Japan) (Supplementary Figure 1). Detailed information of each experiments was provided in Supplementary file. Cancer cell lines: A-549 (human lung carcinoma), SGC-7901 (human stomach carcinoma), PC-3 (human prostate carcinoma), 4T1 (mouse mammary carcinoma), MDA-453 (human breast carcinoma) and MCF-7 (human breast carcinoma) were obtained from the American-Type culture collection (America). MCF-7/ADR (Adriamycin-selected human breast tumor cell line with the MDR phenotype of P-gp overexpression), HUVEC (human umbilical vein endothelial cells) and RAW264.7 (murine macrophage cells) were kindly given by Y Wang, Soochow University (Jiangsu, China). All primary antibodies for WB analysis were purchased from Cell Signaling Technology (MA, USA). All other chemicals and reagents were purchased from Sigma (MO, USA) unless otherwise specified.

Experimental animals

All experiments were performed in accordance with the approval and guidelines of the Ethics Review Committee of Dalian University of Technology. The 5-week-old specific pathogen-free female BALB/c nude mice and BALB/c mice were provided by the Experimental Animal Center at Dalian Medical University, Liaodong, China (SCXK: 2013-0003), and raised and handled under pathogen-free conditions in accordance with the guidelines of the Ethics Committee of Dalian University of Technology.

Caspase detection

Caspase activity was screened using Colorimetric Assay Kit (KeyGEN BioTECH, Nanjing, China) according to the manufacturers instructions. Briefly, MCF-7 cells treated with HN-1 lysed with lysis buffer, and supernatant was collected. Then, caspase substrate was added into protein supernatant for 4 h at 37°C. Absorption at 405 nm was recorded on a microplate reader (Thermo Fisher Scientific, NC, USA). To further validate the effect of caspases in cell death induced by HN-1, MCF-7 cells were treated with HN-1 of $1 \times IC_{50}$, $1.5 \times IC_{50}$ in the presence and absence of caspase-inhibitor z-VAD-fmk (KeyGEN BioTECH), and incubated at 37°C for 12 h. Then the cytotoxicity was measured by MTT described above. Adriamycin (ADR) was used as positive control, which is a commonly used chemotherapy drug and induces the caspase-dependent apoptosis in some cancer cells [32].

Western blotting

The isolation of nuclear, cytosolic and whole-cell protein of MCF-7 cells treated with HN-1 were carried out using Nuclear and Cytoplasmic Protein Extraction Kit (Beyotime Biotechnology, Jiangsu, China) and Whole-cell

Protein Extraction Kit (GL Biochem Ltd, Shanghai, China), respectively. Equal amount of proteins was resolved by SDS-PAGE followed by a standard western blotting procedure.

RNA interference & Bcl-2 overexpression

The predesigned target-specific siRNAs which were used to lower the expression of p53, Bax, AIF and the Bcl-2 expression vector (pEX-2) were purchased from GenePharma (Suzhou, China). siRNAs or purified plasmids were transfected into MCF-7 cells using HieffTrans™ Liposomal Transfection Reagent (Yeasen, Shanghai, China).

Immunofluorescence

After HN-1-treatment, MCF-7 cells on coverslips were fixed with 4% (v/v) paraformaldehyde for 15 min, then covered with 0.3% Triton X-100 and blocked with 5% bovine serum albumin in phosphate-buffered saline (PBS) for 1 h at room temperature. The cells were then incubated with AIF antibody at 4°C overnight, followed by incubation with Alexa Fluor 488-conjugated secondary antibody (KeyGEN, Nanjing, China) for 1 h at room temperature. The nuclei were stained by 4'6-diamidino-2-phenylindole (DAPI, KeyGEN, Nanjing, China). Finally, the stained cells were analyzed using a confocal fluorescence microscope (Olympus, Tokyo, Japan).

In vivo nude mice study

A total of 12 nude mice were implanted subcutaneously with 17 β -estradiol (E2) pellet (1.7 mg, 60-day release, produce 0.3–0.4 nmol/l E2 Blood level) (Innovative Research of America, FL, USA) followed by sealing of the incision with tissue adhesive Vettbond. Then the nude mice were given subcutaneous injection of MCF-7 cells (3×10^6 cells per mouse) into the mammary fat site. After tumors had established ($\sim 50 \text{ mm}^3$), nude mice were assigned equally to two groups (6 animals per group). A total of 100 μl of PBS (as the control group), HN-1 (4 mg/kg in PBS) were given via intraperitoneal (ip.) injection every other day. After transplantation, the body weight and tumor sizes of all mice were recorded every other day. Tumor size was measured with Vernier calipers and calculated as ($[\text{length} \times \text{width}^2]/2$). After 35 days of treatment, mice were sacrificed and the tumors were obtained, photographed and weighted. The tumor and internal organs (heart, lung, kidney, liver and spleen) were fixed in 4% paraformaldehyde (PFA) for immunofluorescence and hematoxylin & eosin (H&E) assay.

In vivo BALB/c mice study

A total of 24 BALB/c mice were given subcutaneous injection of 4T1 cells (3×10^5 cells per mouse) into the mammary fat pad and were divided into four groups once tumor reached a size of 50 mm^3 . Then mice were ip. injected every other day with one of the following treatments: vehicle, PBS, HN-1 (4 mg/kg) and ADR (1 mg/kg). The body weight, tumor sizes, mice sacrifice and internal organs were recorded as nude mice. Spleen cell and blood samples in each group were collected to estimate CD4 $^+$ /CD8 $^+$ T cells percentage and serum cytokine levels, respectively. Tumor sections were used to detect the recruitment of immune cells by immunohistochemistry.

In vivo real-time fluorescent imaging

FITC-labeled HN-1 (FITC-HN-1) was synthesized with the purity >95% (GL Biochem Ltd.). After anesthesia, BALB/c mice bearing 4T1 xenograft tumor were given with 100 μl of FITC-HN-1 (4 mg/kg) through ip. injection. Then the imaging of mice was carried out on a NightOWL II LB983 small animal *in vivo* imaging system with a 495 nm excitation laser and a 519 nm emission filter.

Data analysis

Results were expressed as mean \pm standard error of the mean (SEM) of multiple experiments, unless otherwise specified. Statistical analysis was conducted with an ANOVA followed by the Tukey *t*-test using GraphPad Prism 5.0 software. IC₅₀ were executed by SPSS software. The following indications of significance were used throughout the manuscript: * $p < 0.05$, ** $p < 0.01$ and *** $p < 0.001$.

Results

In vitro & *in vivo* tumor sensitivity to HN-1

HN-1 markedly inhibited multiple tumor cells (A-549, SGC-7901, PC-3, MDA-453, MCF-7 and 4T1) proliferation *in vitro* in a dose-dependent manner with IC₅₀ values ranging from 6.9 to 14.5 μM (Figure 1A, Supplementary Table 1). MCF-7 breast cancer cell showed the most sensitivity to HN-1 treatment with IC₅₀ as low as 6.9 μM

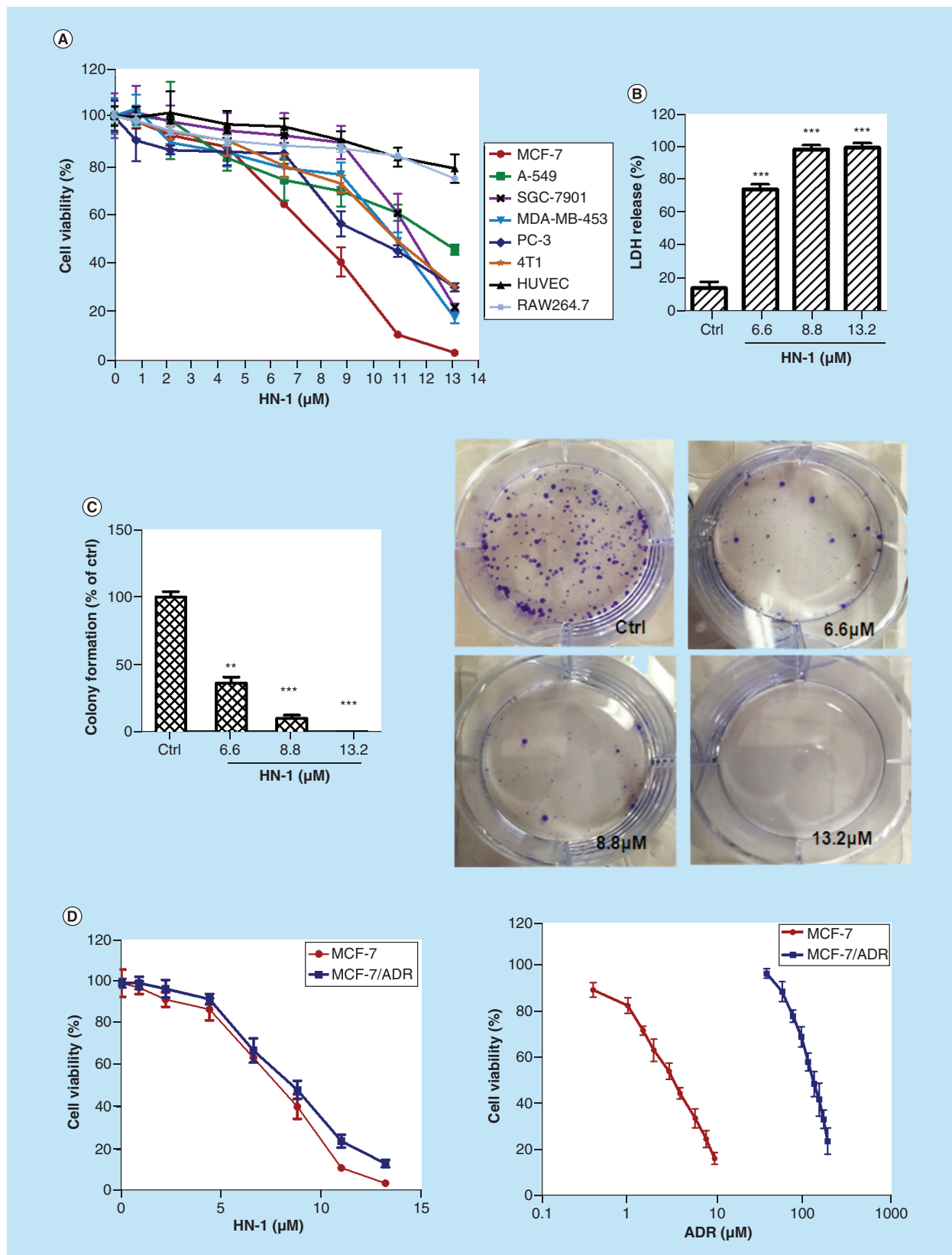


Figure 1. HN-1 inhibited proliferation of multiple malignant cells as well as chemoresistant MCF-7/Adriamycin cell *in vitro*. **(A)** Effects of 48-h treatment of HN-1 on viability of six cancer cells and two normal cells using MTT. Cytotoxicity of HN-1 against MCF-7 cells was estimated by **(B)** lactate dehydrogenase activities and **(C)** clonogenic assays. **(D)** Inhibition effects of HN-1 and ADR on MCF-7 and MCF-7/ADR cells. Data are shown as mean \pm standard error of the mean of three independent experiments.

** $p < 0.01$; *** $p < 0.001$ by Tukey's *t*-test.

ADR: Adriamycin.

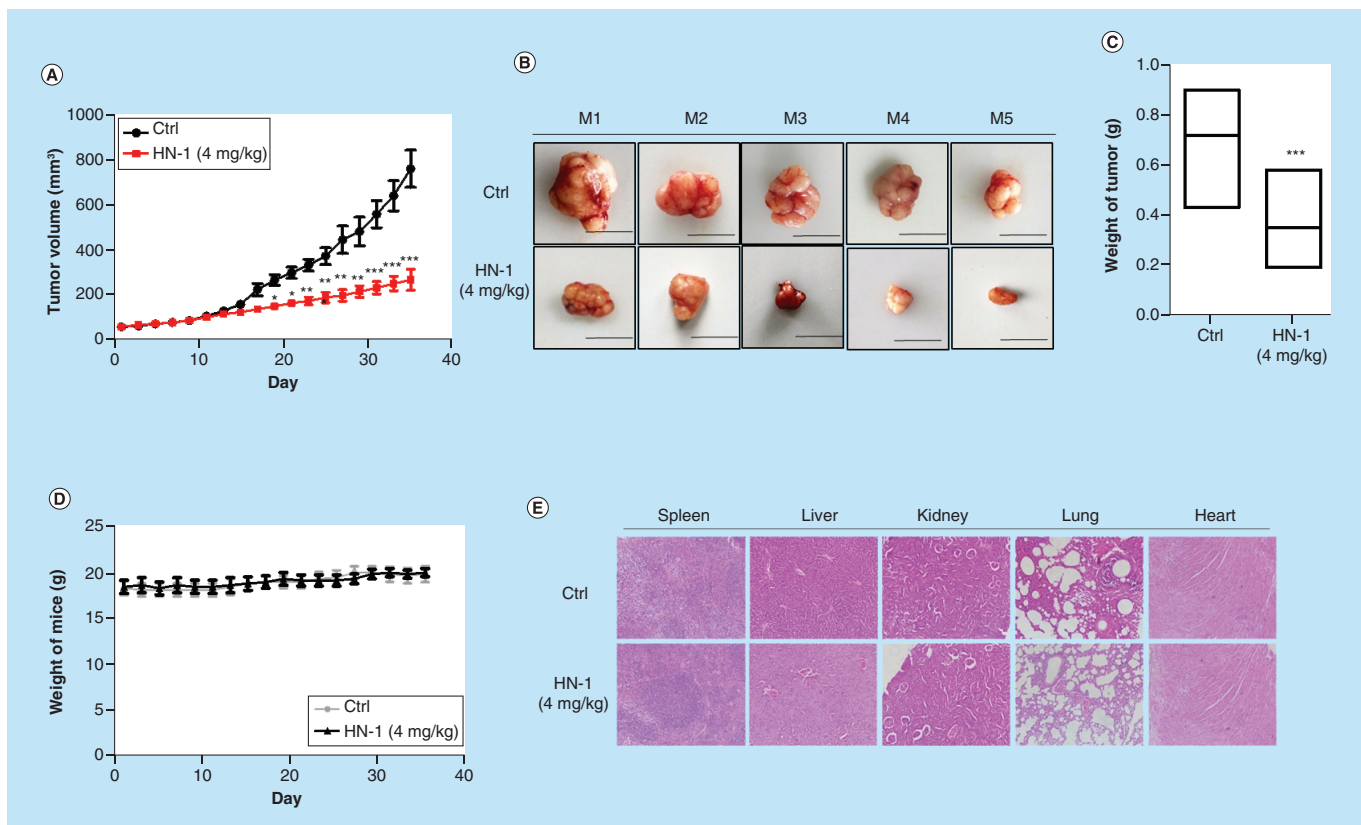


Figure 2. HN-1 inhibited tumor growth and development *in vivo*. Nude mice were inoculated subcutaneously MCF-7 cells, and were ip. injected with PBS (Ctrl) or HN-1 (4 mg/kg) every other day, after the tumors reached approximately 50 mm^3 . **(A)** Mean volume (length \times width 2 /2) of tumor was recorded at the indicated days. **(B)** Volume and **(C)** weight of the tumors removed from sacrificed mice was evaluated after 35 days of treatment. **(D)** The weight of mice was measured every other day. **(E)** Histological data were obtained from the major organs of Ctrl and HN-1-treated nude mice using hematoxylin & eosin staining. M1-4: Mouse 1-4.

(Figure 1B & C). However, HN-1 exhibited relatively little cytotoxicity on HUVEC and RAW264.7 with the values of IC₅₀ six- and seven-times more than MCF-7, respectively (Supplementary Table 1). More importantly, HN-1 also exerted remarkable cytotoxicity against MCF-7/ADR with the IC₅₀ of 8.17 μM , comparable to that of MCF-7 (Figure 1D).

The antitumor efficacy of HN-1 *in vivo* was next evaluated on nude mice xenografted with human MCF-7 cells, which proliferated and rapidly colonized in mice. After the tumors reached a size of approximately 50 mm^3 , ip. administration of HN-1 (4 mg/kg) every other day for 35 days led to a significant decrease in tumor volume by 65.44% (Figure 2A & B). The tumor weight in HN-1-treated groups was significantly reduced to $0.35 \pm 0.06 \text{ g}$ (Figure 2C), whereas the mean body weights for both therapeutic and placebo group did not show significant differences (Figure 2D). *In vivo* toxicology of HN-1 was next evaluated by hematoxylin & eosin staining, which showed no pathological toxicity and adverse effects to the main organs, suggesting no significant histological abnormalities induced by HN-1 (Figure 2E).

HN-1 induced MCF-7 apoptosis without caspase activation

Despite HN-1's direct antineoplastic activity by inducing pore-formation on tumor cell membranes (Figure 3A), which is ascribed to its highly positive charge and typical amphipathic α -helical conformation (Figure 3B), HN-1 also triggered apoptosis in MCF-7 cells detected by flow cytometry (Figure 4A). Likewise, HN-1 treatment led to nuclear fragmentation and chromatin condensation in MCF-7 cells as shown by DAPI staining (Figure 3B) and TUNEL assay, showing a 63.4% TUNEL positive cells (Figure 4C). Furthermore, similar with the mitochondrial poison CCCP, MCF-7 cells treated with HN-1 showed a decrease by more than 60% in fluorescence signal stained by rhodamine 123 (Figure 4D), suggesting a breakdown in ΔYm . Activation of caspases and the subsequent

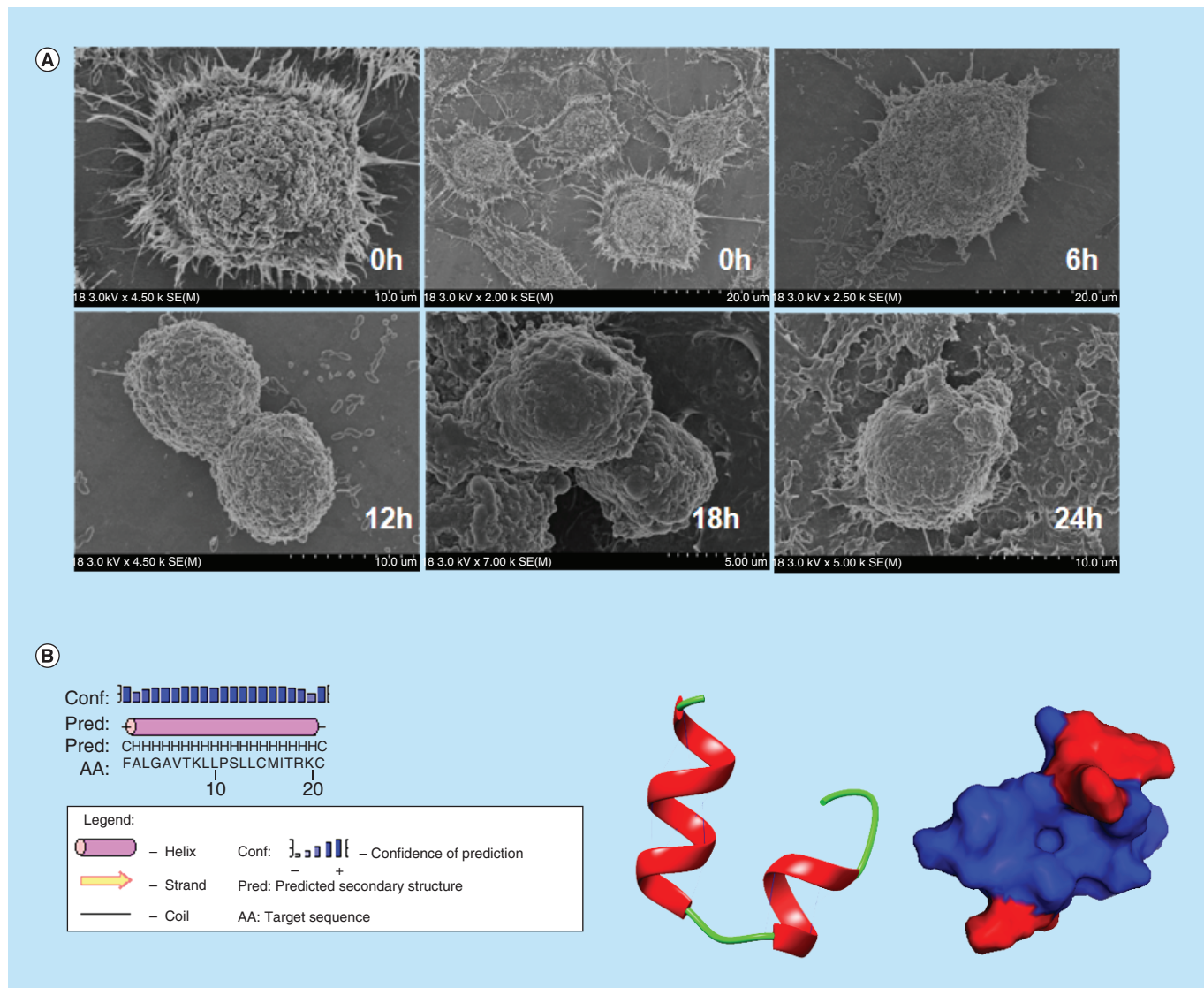


Figure 3. Morphological changes induced by HN-1 in MCF-7 cells and structure of HN-1. (A) Standard error of the mean images of cells treated with $1 \times IC_{50}$ of HN-1 for 0, 6, 12, 18 and 24 h. **(B)** Secondary structure predicted by PSIPRED v3.3 and built by Rosetta *ab initio* of HN-1. For the latter, intramolecular hydrogen bonds and α -helix are displayed in the ribbon structure. Surface representation of HN-1 is shown in blue with positive charges shown in red region.

cleavage of PARP are characteristic of cell apoptosis [33]. Unexpectedly, 12-h HN-1 treatment did not cause the distinct activation of caspase-1, -3, -8 and -9, and cleavage of PARP as ADR (Figure 4E), hinting at the possibility that HN-1 induced apoptotic cell death in a caspase-independent manner. This hypothesis was substantiated by the finding that the pan-caspase inhibitor z-VAD-fmk failed to reverse the MCF-7 cell apoptosis induced by HN-1 (Figure 4F).

HN-1 triggered nuclear translocation of AIF both *in vitro* & *in vivo* to mediate apoptosis

In caspase-independent apoptosis, a mitochondrial-localized protein, AIF (apoptosis-inducing factors), would translocate from the mitochondria to the nucleus to cause chromatin condensation and DNA degradation [34]. In Figure 5A, after treatment with $1 \times IC_{50}$ of HN-1 for 0, 3, 6, 12, 24 h, the nuclear protein level of AIF was gradually increased, and peaked at 12 h, whereas its cytosolic level was inversely decreased. The change of subcellular localization of AIF activated by HN-1 was further confirmed by immunofluorescence, showing a redistribution of AIF from the cytosol to the nucleus in response to HN-1 treatment (Figure 5B). RNA interference (RNAi) was

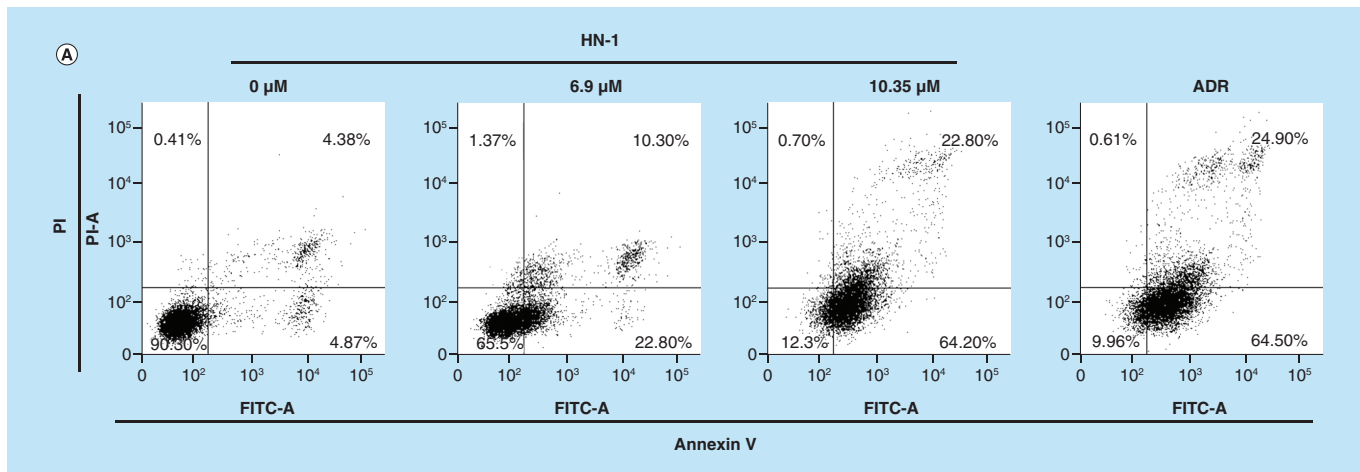


Figure 4. HN-1 induced caspase-independent apoptosis in cancer cells. (A) Flow cytometry analysis of Annexin V/PI-stained MCF-7 cells treated with phosphate-buffered saline (Ctrl), HN-1 or Adriamycin. **(B)** The nucleolus morphologic changes observed in MCF-7 cells treated with HN-1. **(C)** Apoptosis of MCF-7 cells confirmed by TUNEL staining. **(D)** Mitochondrial membrane potential ($\Delta\Psi_m$) alterations in MCF-7 cells detected by flow cytometry, CCCP as positive control. **(E)** Cleaved caspase-3, -8 and -9 and PARP examined in MCF-7 cells treated with $1 \times IC_{50}$, $1.5 \times IC_{50}$ HN-1 or $1.5 \times IC_{50}$ ADR by spectrophotometry analysis and western blot. **(F)** Pan-caspase inhibitor z-VAD-fmk ($20 \mu\text{mol/l}$) failed to reverse the loss of cell viability-induced HN-1 as measured by MTT. Each value is the mean \pm standard error of the mean of three determinations.

** $p < 0.01$; *** $p < 0.001$ significantly different from respective control group.
ADR: Adriamycin.

used to knock down AIF expression to further determine its role in HN-1-induced apoptosis, and results showed that transfection with AIF-siRNA significantly reduced nuclear protein levels (Figure 5C), and reversed the tumor cells death caused by HN-1 *in vitro* (Figure 5D & E). *In vivo*, AIF nuclear translocation was also observed in tumor biopsies from HN-1 treated xenografts determined by WB (Figure 5F) and immunofluorescence staining (Figure 5G). Altogether, HN-1 triggered migration of AIF from the mitochondria to the nucleus to mediate caspase-independent apoptosis.

HN-1 activated p53 & altered the expression of Bcl-2 family members in AIF-mediated apoptosis

Bcl-2 family members are important mediators in the mitochondrial apoptosis [35]. In this regard, HN-1 was found upregulating the pro-apoptotic Bax and apparently decreasing the anti-apoptotic Bcl-2 levels in MCF-7 cells (Figure 6A), both most prominently at 12-h post-treatment. Further, the nuclear translocation of AIF induced by HN-1 was reversed by knockdown of Bak, and/or overexpression of Bcl-2 in MCF-7 (Figure 6B), followed by the completely loss of apoptotic effect by HN-1 (Figure 6C & D). Altogether, upregulation of Bax and downregulation of Bcl-2 were required in caspase-independent tumor cell apoptosis triggered by HN-1.

The tumor-suppressor protein p53 has been demonstrated to regulate both caspase-dependent and -independent apoptosis in a wide variety of biologic contexts [36]. As shown in Figure 6E, total and nuclear protein levels of p53 in HN-1-treated MCF-7 were increased and peaked at 12 h, which preceded the altered expression of Bax and Bcl-2 (Figure 6F) and upregulated modulator of apoptosis (PUMA), a direct target gene of p53 (Figure 6E). To investigate whether the altered expression of Bcl-2 family members caused by HN-1 was p53-dependent, we used siRNA to silence p53 in MCF-7. Knockdown of p53 significantly reversed the induction of Bax as well as the downregulation of Bcl-2 induced by HN-1, and subsequently the increase in the nuclear expression of AIF (Figure 6F) and cell survival (Figure 6G). Similarly, the increased Bax and decreased Bcl-2 were both observed in xenograft tumors in nude mice after HN-1 treatment (Figure 6H).

MAPK/NF-κB signaling pathway was involved in HN-1 induced cancer cell apoptosis both *in vitro* & *in vivo*

Reactive oxygen species (ROS) acts as important signaling molecules in inducing depolarization of the mitochondrial membrane, and consequently cancer cell apoptosis [37]. To measure the O_2^- and H_2O_2 levels induced by HN-1 for initiation the apoptosis, MCF-7 cells were stained with DHE and H2DCFDA probe, respectively. Both flow

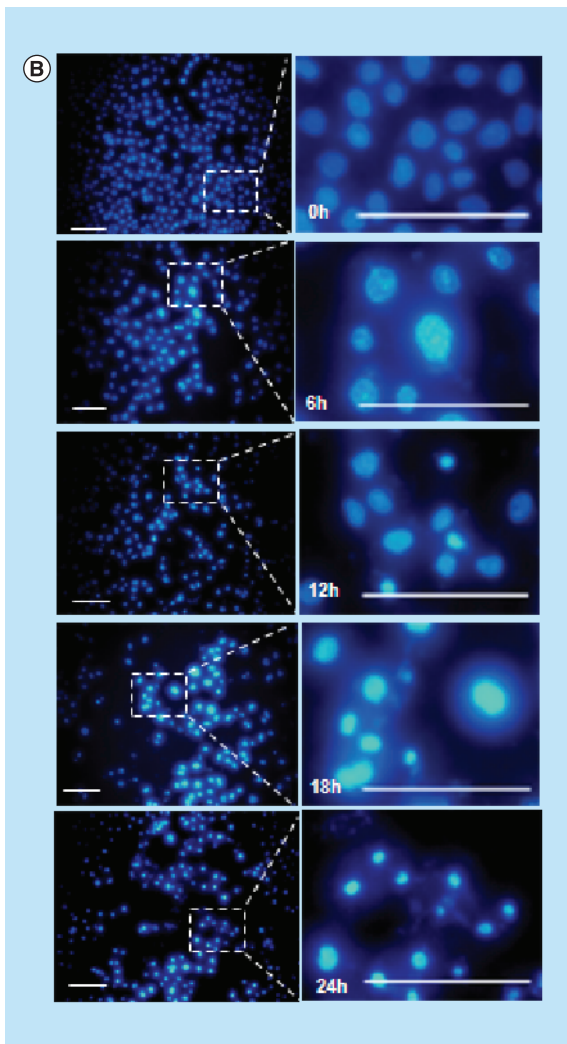


Figure 4. HN-1 induced caspase-independent apoptosis in cancer cells (cont.). (A) Flow cytometry analysis of Annexin V/PI-stained MCF-7 cells treated with phosphate-buffered saline (Ctrl), HN-1 or Adriamycin. (B) The nucleolus morphologic changes observed in MCF-7 cells treated with HN-1. (C) Apoptosis of MCF-7 cells confirmed by TUNEL staining. (D) Mitochondrial membrane potential ($\Delta\Psi_m$) alterations in MCF-7 cells detected by flow cytometry, CCCP as positive control. (E) Cleaved caspase-3, -8 and -9 and PARP examined in MCF-7 cells treated with $1 \times IC_{50}$, $1.5 \times IC_{50}$ HN-1 or $1.5 \times IC_{50}$ ADR by spectrophotometry analysis and western blot. (F) Pan-caspase inhibitor z-VAD-fmk ($20 \mu\text{mol/l}$) failed to reverse the loss of cell viability-induced HN-1 as measured by MTT. Each value is the mean \pm standard error of the mean of three determinations.
** $p < 0.01$; *** $p < 0.001$ significantly different from respective control group.
ADR: Adriamycin.

cytometer and fluorescence microscope indicated the increases of H2DCFDA and DHE-derived fluorescence after HN-1 treatment (Figure 7A). ROS-induced apoptosis is always associated with activation of MAPK signaling pathways [38]. Similarly, HN-1 induced an activation of p38 and JNK1/2 in MCF-7 cells in a time-dependent manner, while markedly attenuated phosphorylation level of ERK1/2 that generally promotes cell survival [39] (Figure 7B). HN-1 decreased the degradation of I κ B α in cytoplasm and subsequently the nuclear translocation of NF- κ B (Figure 7C), which plays an important role in tumor promotion and progression and anti-apoptosis [40]. Consistently, HN-1 increased the p-p38 and p-JNK1/2, and decreased the p-ERK1/2 levels in xenograft tumors in nude mice as well (Figure 7D).

HN-1 induced anticancer immunity in a 4T1 murine breast cancer model without systemic toxicity
In order to determine whether HN-1 stimulates host anticancer immunity to cooperate for tumor eradication, we established a 4T1 breast cancer models in BALB/c mice. HN-1 and ADR effectively suppressed the tumor growth with inhibition rates of 64.4 and 41.6%, respectively, after 35-day treatment (Figure 8A). Both the tumor volume and weight in HN-1 group were significantly smaller than the vehicle and ADR group (Figure 8B). Mean body weight did not show any significant differences from those of vehicle group (Figure 8C). The spleen index commonly used to assess the splenic size for HN-1 group was much smaller than that of the tumor ($p < 0.01$) and ADR groups ($p < 0.05$) (Figure 8D). As shown in Figure 8E, tumor metastasis and filtration of inflammatory cells were observed in tumor group. However, HN-1 markedly reduced the infiltration of inflammatory cell-related tumor metastasis in lung, liver and spleen without notable visceral toxicity, while the histological images from H&E staining showed that ADR partly destroyed heart structure, and failed to prevent the tumor metastasis (Figure 8E).

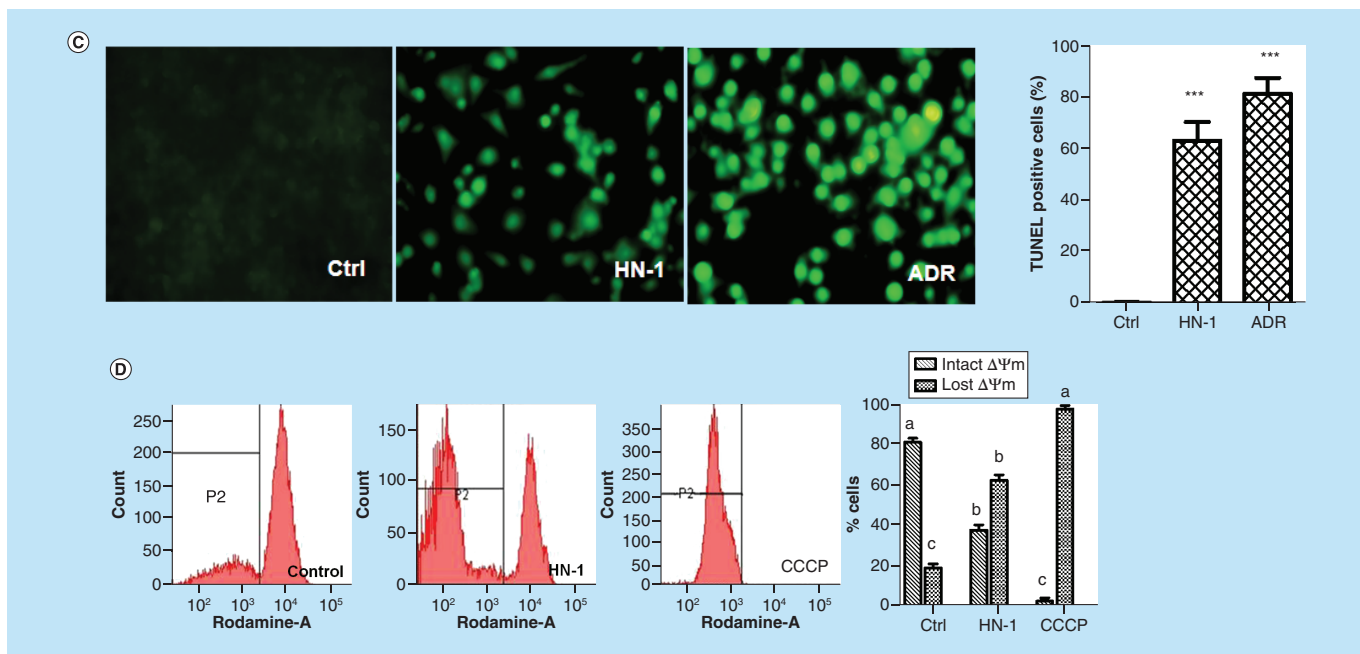


Figure 4. HN-1 induced caspase-independent apoptosis in cancer cells (cont.). (A) Flow cytometry analysis of Annexin V/PI-stained MCF-7 cells treated with phosphate-buffered saline (Ctrl), HN-1 or Adriamycin. (B) The nucleolus morphologic changes observed in MCF-7 cells treated with HN-1. (C) Apoptosis of MCF-7 cells confirmed by TUNEL staining. (D) Mitochondrial membrane potential ($\Delta\Psi_m$) alterations in MCF-7 cells detected by flow cytometry, CCCP as positive control. (E) Cleaved caspase-3, -8 and -9 and PARP examined in MCF-7 cells treated with $1 \times IC_{50}$, $1.5 \times IC_{50}$ HN-1 or $1.5 \times IC_{50}$ ADR by spectrophotometry analysis and western blot. (F) Pan-caspase inhibitor z-VAD-fmk ($20 \mu\text{mol/l}$) failed to reverse the loss of cell viability-induced HN-1 as measured by MTT. Each value is the mean \pm standard error of the mean of three determinations.

p < 0.01; *p < 0.001 significantly different from respective control group.

ADR: Adriamycin.

Cancer immunity involves detection of cancer cells at an early stage, and the subsequent immunomodulation of immune cells including NK cells, CD4⁺ and CD8⁺ lymphocytes, regulatory T cells, TAMs and dendritic cells, etc [41]. IL-2 stimulates the proliferation and effector function of cytotoxic T lymphocytes (CTLs) and NK cells [42]. TNF- α acts as a T lymphocytes differentiation factor and B-cell activator [43], in addition to direct antineoplastic effector. IL-12 enhances NK and T-cell activation and IFN- γ production, which induces T-cell differentiation into a Th1-type [44], and IL-10 downregulates IFN- γ production and in turn affects T-cell differentiation [45]. The chemokine MCP-1 modulates macrophages/monocytes trafficking to tumor cells, and potentiates their cytotoxic functions [46]. Herein, the levels of serum chemokine and cytokines were analyzed in mice after 24-h treatment. Results showed that HN-1 significantly enhanced the level of all serum cytokine/chemokine tested, especially to IL-2 and IFN- γ that are important in T-cell activation and differentiation, compared with ADR (Figure 8F), whereas the level of IL-10 was not altered in a statistically significant way.

We next compared CD4⁺ and CD8⁺ T cell amounts in splenocyte isolates from nonimmunized (vehicle) and immunized mice (4T1 tumor cells alone, 4T1+HN-1 and 4T1+ADR). HN-1 significantly increased CD4⁺ T cell percentage compared with the other three groups ($p < 0.05$), and fairly elevate CD8⁺ T cell amount (Figure 8G, Supplementary Table 2), suggesting the capability of HN-1 to eradicate tumor by virtue of its modulating the tumor-associated immune response. In addition, tumor progression especially in late stage usually involves angiogenesis, as well as TAMs infiltrating solid tumors that exert a protumorigenic function by immune-suppressing NK and T cells [47]. Immunohistochemistry with cell surface marker antibodies revealed that HN-1 enhanced the infiltration of CD4⁺ T cells, but significantly decreased TAMs that typically promote cancer metastasis, and prevented the blood capillary formation, as evidenced by decreases of VEGF (Figure 8H).

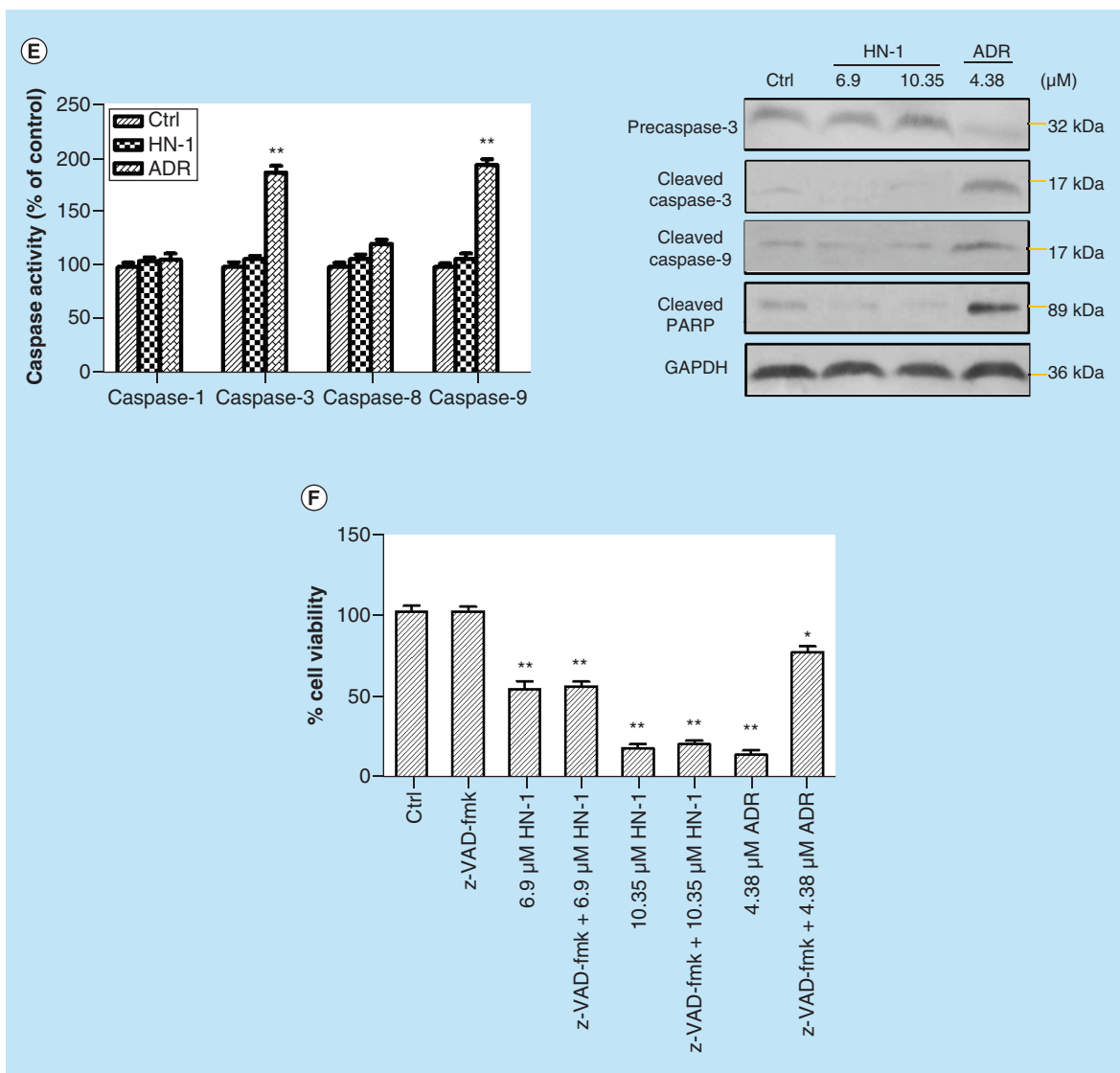


Figure 4. HN-1 induced caspase-independent apoptosis in cancer cells (cont.). (A) Flow cytometry analysis of Annexin V/PI-stained MCF-7 cells treated with phosphate-buffered saline (Ctrl), HN-1 or Adriamycin. (B) The nucleolus morphologic changes observed in MCF-7 cells treated with HN-1. (C) Apoptosis of MCF-7 cells confirmed by TUNEL staining. (D) Mitochondrial membrane potential ($\Delta\psi_m$) alterations in MCF-7 cells detected by flow cytometry, CCCP as positive control. (E) Cleaved caspase-3, -8 and -9 and PARP examined in MCF-7 cells treated with $1 \times IC_{50}$, $1.5 \times IC_{50}$ HN-1 or $1.5 \times IC_{50}$ ADR by spectrophotometry analysis and western blot. (F) Pan-caspase inhibitor z-VAD-fmk (20 μ mol/l) failed to reverse the loss of cell viability-induced HN-1 as measured by MTT. Each value is the mean \pm standard error of the mean of three determinations.
** $p < 0.01$; *** $p < 0.001$ significantly different from respective control group.
ADR: Adriamycin.

In vivo biodistribution of HN-1 in tumor-bearing mice

To track the biodistribution of HN-1, the spontaneous fluorescence of FITC-labeled HN-1 (FITC-HN-1) was analyzed both in mice and in tissue sections using NightOWL II LB983 small animal *in vivo* imaging system. Fluorescence signals gradually distributed to epigastrium from the injection site, but were too weak for direct observations in specific tissue (Figure 9A). While *ex vivo*, bright specific FITC-HN-1 fluorescence was observed exemplarily in tumor, spleen, intestine, kidney and bladder, (Figure 9B), among which bladder as main excretion organ showed the strongest signal. A rapid and large accumulation of HN-1 in tumor revealed a good tumor target

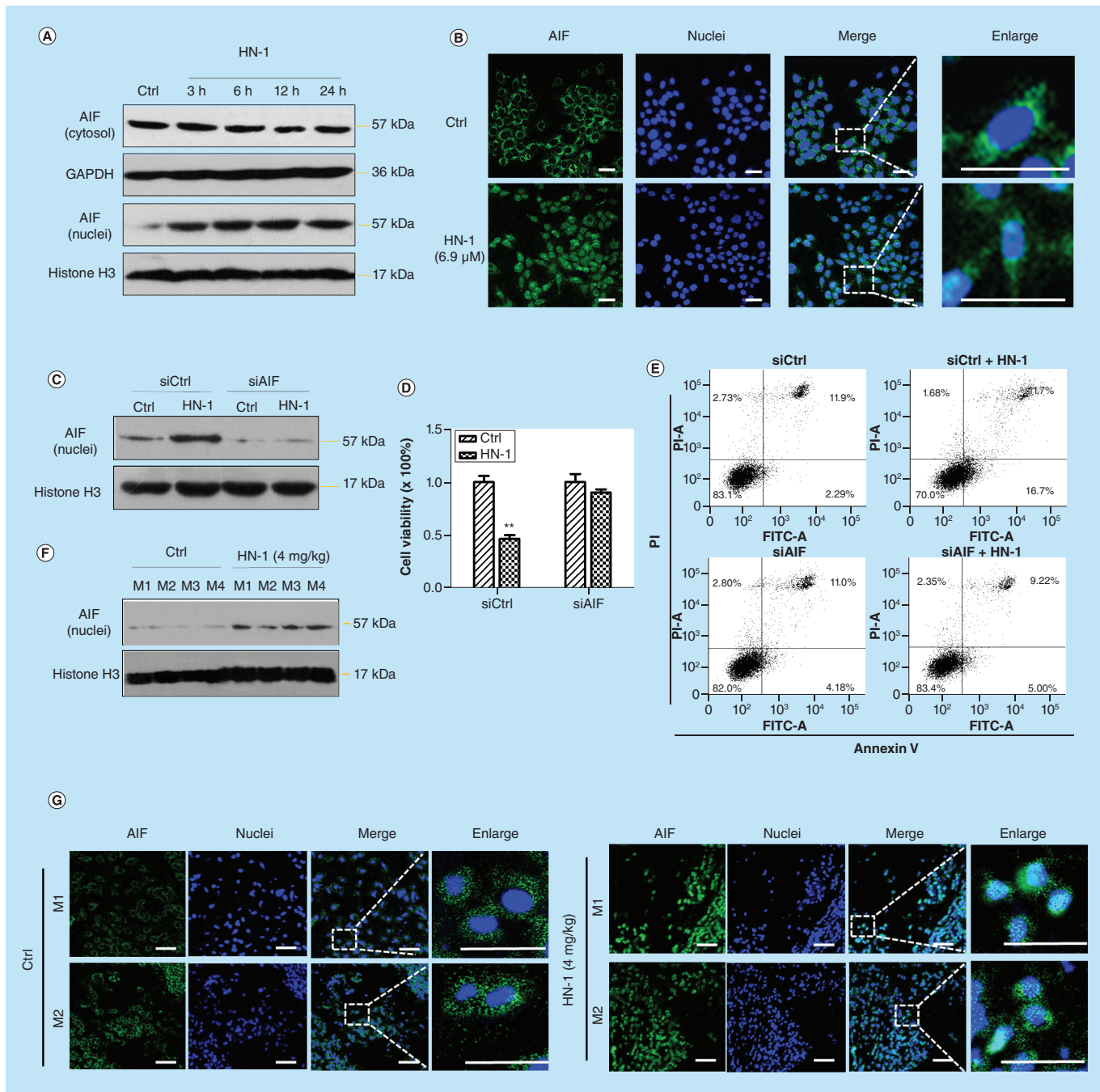


Figure 5. HN-1-triggered nuclear translocation of AIF both *in vitro* and *in vivo* in mediating apoptosis. **(A)** Cytosolic and nuclear levels of AIF in MCF-7 cells with $1 \times IC_{50}$ of HN-1 treatment for 0, 3, 6, 12, 24 h determined by western blot. **(B)** The nuclear translocation of AIF treated with or without HN-1 observed by immunofluorescence. AIF-siRNA was transfected into MCF-7 cells followed by 12-h HN-1 treatment. **(C)** Then the nuclear expression of AIF was determined by western blot, **(D)** cell viability was detected by MTT, **(E)** and apoptosis was detected by Annexin V/PI staining. **(F)** Nuclear expression and **(G)** subcellular localization of AIF in breast tumors xenograft in nude mice were determined by western blot analysis and immunofluorescence, respectively. GAPDH and Histone H3 were used as equal loading controls for cytosolic and nuclear proteins, respectively. Data are shown as mean \pm standard error of the mean of three independent experiments.

** $p < 0.01$ by Tukey's *t*-test.

M1-4: Mouse 1-4.

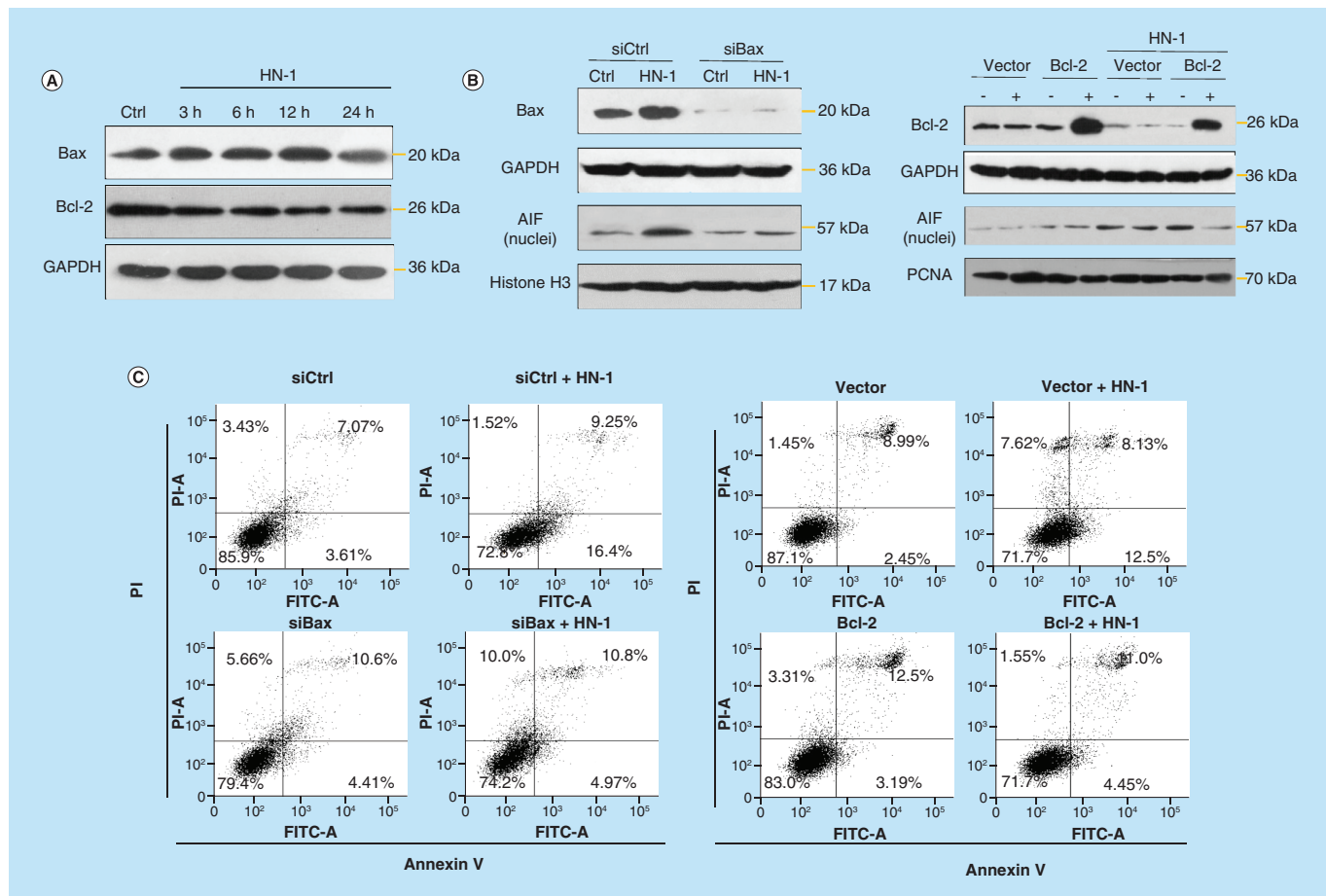


Figure 6. Activated p53 and altered expression of Bcl-2 family members were required in HN-1-induced AIF-mediated apoptosis. (A) HN-1 increased Bax but decreased Bcl-2 expression, which were peaked at 12 h after treatment. Knockdown of Bax and overexpression of Bcl-2 reduced HN-1-induced nuclear translocation of AIF by western blot (B), and tumor cell apoptosis by (C) flow cytometry and (D) MTT assay. (E) Total and nuclear levels of p53 together with PUMA were upregulated in HN-1-treated MCF-7. (F) Knockdown of p53 abolished the upregulation of Bax and downregulation of Bcl-2 as well as the nuclear translocation of AIF induced by HN-1. (G) The tumor cell apoptosis was reversed by blocking p53 in HN-1-treated MCF-7. (H) Alterations of Bcl-2 family members in breast tumor xenograft in nude mice after HN-1 treatment were also consistent with the *in vitro* results. Data are shown as mean \pm standard error of the mean of three independent experiments.

** $p < 0.01$ by Tukey's *t*-test.

M1-4: Mouse 1-4.

of HN-1, thereby, resulting in enhanced antitumor effects and decreased drug accumulation in normal tissues. Remarkably, no fluorescence was detected in heart, lung and liver, confirming safety of HN-1 to main organs.

Discussion

During the past several decades, cancer treatment has evolved from relatively nonspecific chemotherapy to selective, mechanism-based targeted therapies. However, effect of chemotherapy is weakened by significant toxicities, narrow therapeutic index and frequently acquired resistance, although it remains a backbone of current treatment paradigm. Targeted treatments aiming the critical molecular pathways in tumor growth and maintenance may elicit dramatic but generally short-lived tumor regressions, limiting the overall clinical benefit. More recently, a great deal of clinical trial successes indeed validated the practicability of immunotherapy that attempts to stimulate host response, albeit it is associated with a significant incidence of inflammatory toxicities [17]. Chemo- and targeted agents are also found modulating immune responses, which gives rise to the possibility to improve clinical outcomes by effective combining the two strategies.

In the present study, we have identified a HDP, HN-1, which can markedly inhibit proliferation of various malignant cell lines: A-549, SGC-7901, PC-3, 4T1, MDA-453 and MCF-7 *in vitro*. In addition, HN-1 was also

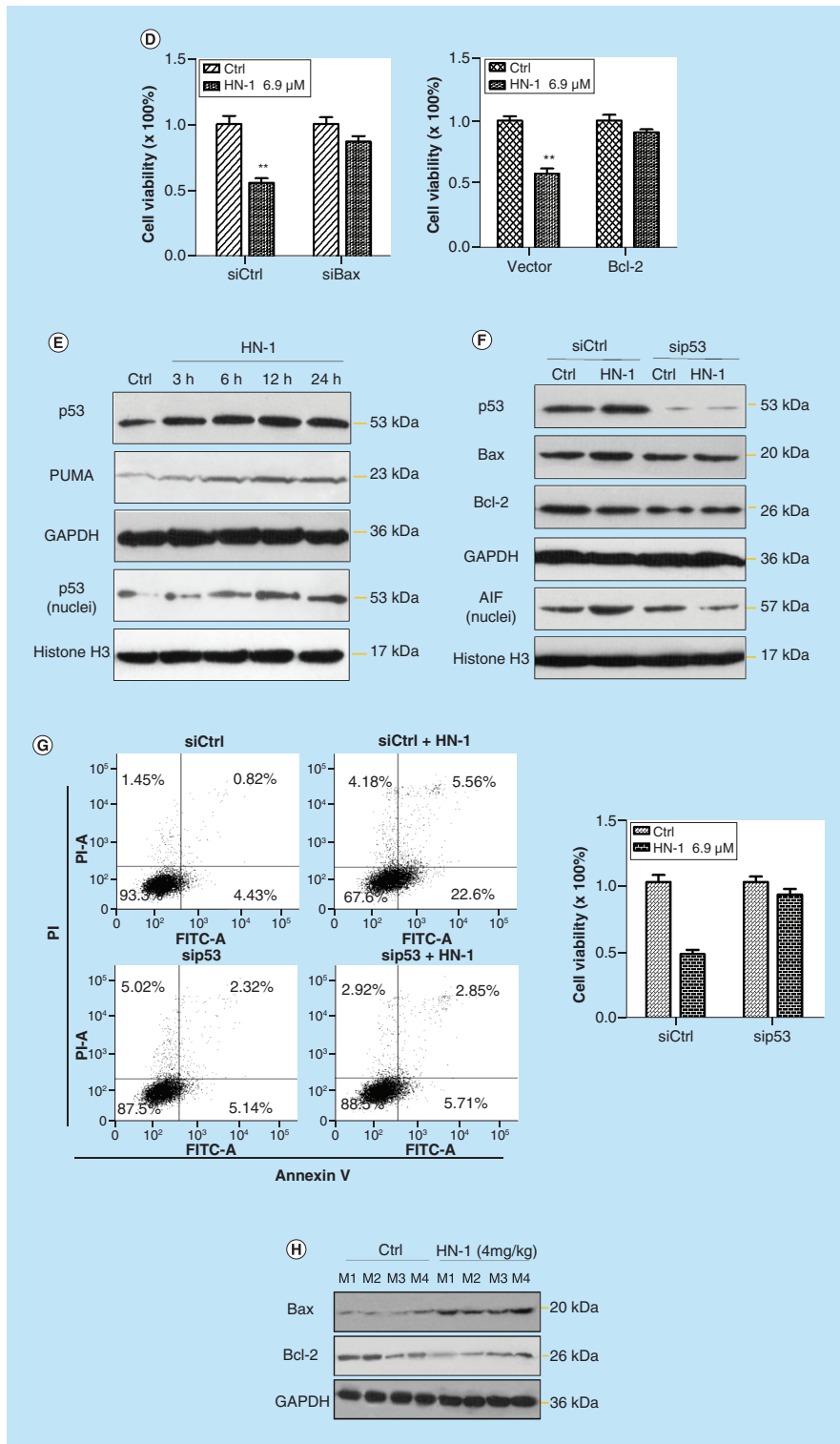


Figure 6. Activated p53 and altered expression of Bcl-2 family members were required in HN-1-induced AIF-mediated apoptosis (cont.). (A) HN-1 increased Bax but decreased Bcl-2 expression, which were peaked at 12 h after treatment. Knockdown of Bax and overexpression of Bcl-2 reduced HN-1-induced nuclear translocation of AIF by western blot (B), and tumor cell apoptosis by (C) flow cytometry and (D) MTT assay. (E) Total and nuclear levels of p53 together with PUMA were upregulated in HN-1-treated MCF-7. (F) Knockdown of p53 abolished the upregulation of Bax and downregulation of Bcl-2 as well as the nuclear translocation of AIF induced by HN-1. (G) The tumor cell apoptosis was reversed by blocking p53 in HN-1-treated MCF-7. (H) Alterations of Bcl-2 family members in breast tumor xenograft in nude mice after HN-1 treatment were also consistent with the *in vitro* results. Data are shown as mean \pm standard error of the mean of three independent experiments.

** $p < 0.01$ by Tukey's *t*-test.

M1-4: Mouse1-4.

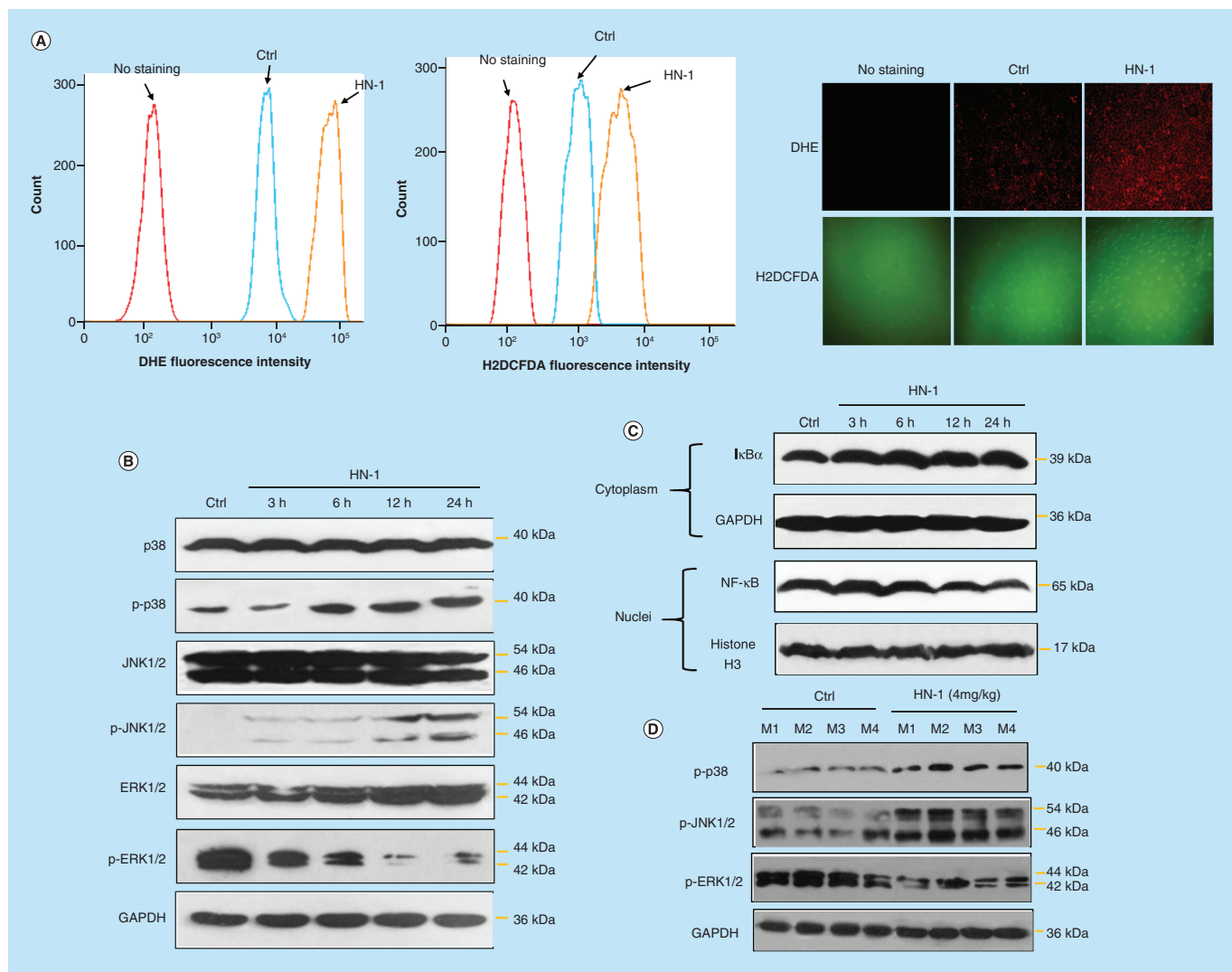


Figure 7. The reactive oxygen species/MAPK/NF- κ B signaling pathway was involved in HN-1-induced apoptotic responses. **(A)** HN-1-treated MCF-7 cells were stained with DHE and H2DCFDA molecular probe for detecting the accumulation of O $_2^-$ and H $_2$ O $_2$ by flow cytometer and fluorescence microscope, respectively. **(B)** Western blot analyses for p-p38, p38, p-JNK/SAPK, JNK/SAPK, p-ERK1/2, ERK1/2, p-ERK1/2, and GAPDH in MCF-7 cells treated with HN-1 for different time periods. **(C)** I κ B α and NF- κ B in MCF-7 cells treated with HN-1 for different time periods. **(D)** HN-1 upregulated level of p-JNK, p-p38 and downregulated level of p-ERK in breast tumor xenograft in nude mice. M1-4: Mouse 1-4.

capable of inducing death in chemo-resistant cancer cell (MCF-7/ADR) *in vitro*, suggesting that HN-1 might be a valuable complement to current chemotherapy without inducing acquired resistance. *In vivo* data also showed that HN-1 notably inhibited tumor growth in a xenograft breast tumor model. Subsequent experiments revealed that HN-1 induced the apoptosis in cancer cells in addition to direct interfering cell membrane integrity, which prompts us to investigate the HN-1's apoptogenic mechanism. It was then demonstrated that unlike most conventional chemotherapeutic agents, HN-1 induced a caspase-independent apoptosis, which has been only reported on human LL-37 in colon tumorigenesis, and cathelicidin HDPs in other cell types, including periodontal ligament cells and infected airway epithelium [25]. For the first time through our investigations, we show that anticancer HDP could act through the caspase-independent pathway to mediate apoptosis in cancer cells, whereas most other anticancer HDPs identified, such as Buforin IIb [48], Lactoferricin B [27] and Pardaxinin [49], induce apoptosis in a caspase-dependent manner. Subsequently, we uncovered that HN-1 induced nuclear translocation of AIF, paralleled by remarkable breakdown in mitochondrial membrane $\Delta\Psi_m$, the upregulation of proapoptotic Bax and the downregulation of anti-apoptotic Bcl-2 *in vitro*. By forming complexes on the outer mitochondrial membrane, Bax facilitates

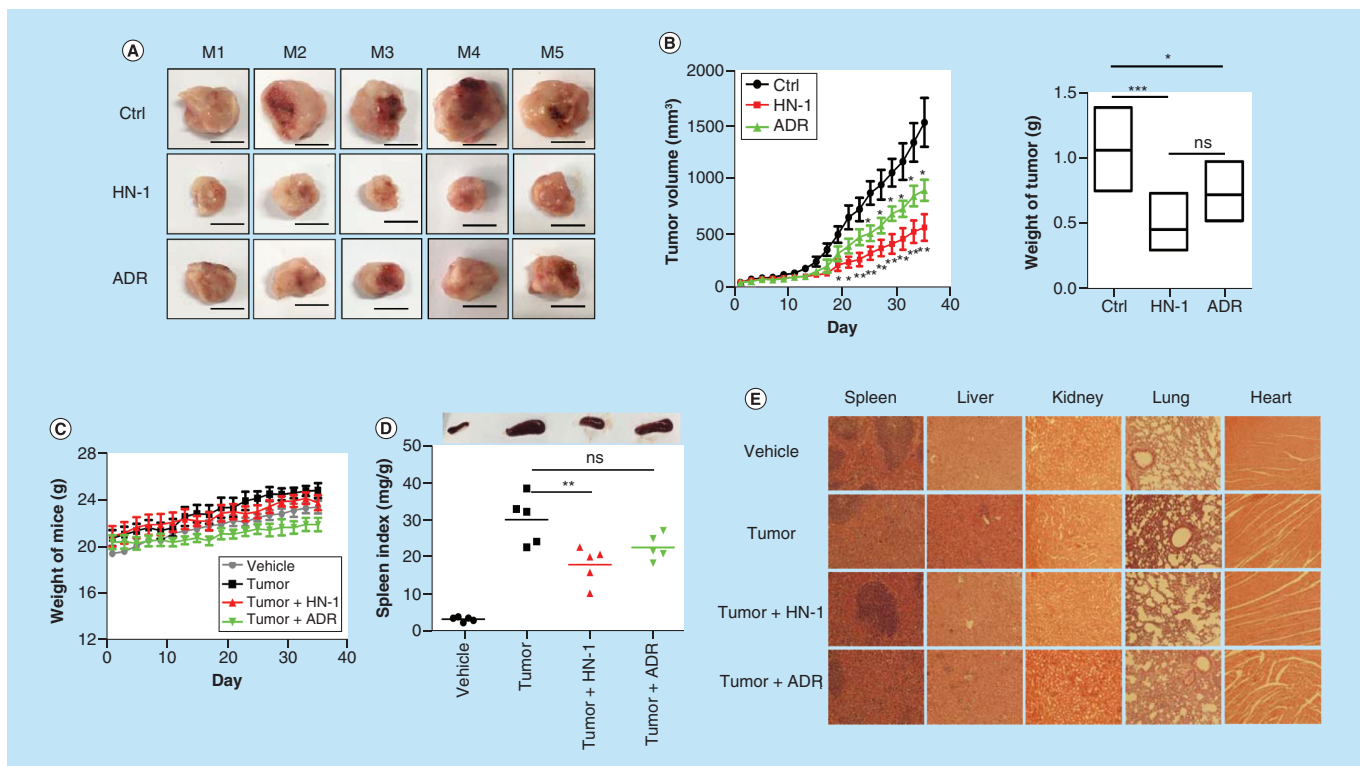


Figure 8. HN-1 inhibited tumor and activated antitumor immune response in a 4T1 murine breast cancer model without causing systemic toxicity. (A, B) HN-1 significantly inhibited the tumor growth in a 4T1 breast cancer models in BALB/c mice, and decreased tumors volume and weight (B). (C) HN-1 did not cause the weight loss of the mice during the treatment. (D) HN-1 dramatically lowered spleen index of tumor-bearing mice. (E) Hematoxylin & eosin staining was used to detect the histological changes of viscera after HN-1 and ADR treatment. (F) HN-1 remarkably increased the serum levels of cancer immunity-associated chemokines and cytokines in BALB/c-derived 4T1 mammary carcinoma model mice, including MCP-1, IL-2, TNF- α , IFN- γ and IL-12, but did not alter the IL-10 level statistically. (G) HN-1 significantly stimulated CD4 $^+$ T-cell proliferation and increased the level of CD4 $^+$ /CD8 $^+$ in spleen. (H) Immunohistochemistry revealed that HN-1 enhanced the infiltration of CD4 $^+$ T cells, and prevented the blood capillary formation, as evidenced by decreases of VEGF, but significantly decreased tumor-associated macrophages in solid tumor. Data are shown as mean \pm standard error of the mean of three independent experiments.

*p < 0.05; **p < 0.01; ***p < 0.001 by Tukey's t-test. Letters on top of the bar charts indicate significant differences between control and experimental group by Duncan's multiple-range test. Tukey: compare pairs of columns.
ADR: Adriamycin; ns: Not significant.

the release of AIF, while Bcl-2 prevents the activation of Bax and the following Bax-mediated cell apoptosis [25]. Consistently, *in vivo* study also showed the altered expression of Bcl-2 family proteins inducing the AIF nuclear translocation in HN-1-treated breast tumor xenografted nude mice.

The tumor suppressor protein, p53 was proved extremely requisite in HN-1-induced caspase-independent apoptosis, since HN-1 increased both whole-cell and nuclear p53 expression, accompanied by induction of PUMA and Bax and reduction of Bcl-2, which was also recapitulated in p53 knockdown cells. ROS generated from cellular oxidative processes may induce depolarization of the mitochondrial membrane, and consequently increase the level of proapoptotic molecules in the cells [37]. Meanwhile, ROS activates the downstream MAPK/NF- κ B signaling cascade, which regulates a diverse range of cellular responses, including cell proliferation, differentiation, mitosis, survival, inflammation and apoptosis [38]. Here, we found that HN-1 apparently enhanced the cellular generation of O₂⁻ and H₂O₂, and induced ROS-dependent activation of JNK and p38 pathways but considerably inhibited ERK1/2 and NF- κ B pathway, both *in vitro* and *in vivo*. MAPKs regulate the relative abundance of the pro- and anti-apoptotic proteins of the Bcl-2 family [50], while NF- κ B, as a chemoresistance-related anti-apoptotic factor, participates in inflammation and tumorigenesis [40]. Together with the Bcl-2 family data presented above, these findings further support a central role of MAPK/NF- κ B in mediating the apoptotic activity of HN-1.

Nowadays, accumulating evidence indicates that combinatorial anticancer therapy combining chemo- or radiotherapeutics with immunotherapy results in synergistic antineoplastic effects. This strategy not only decreases

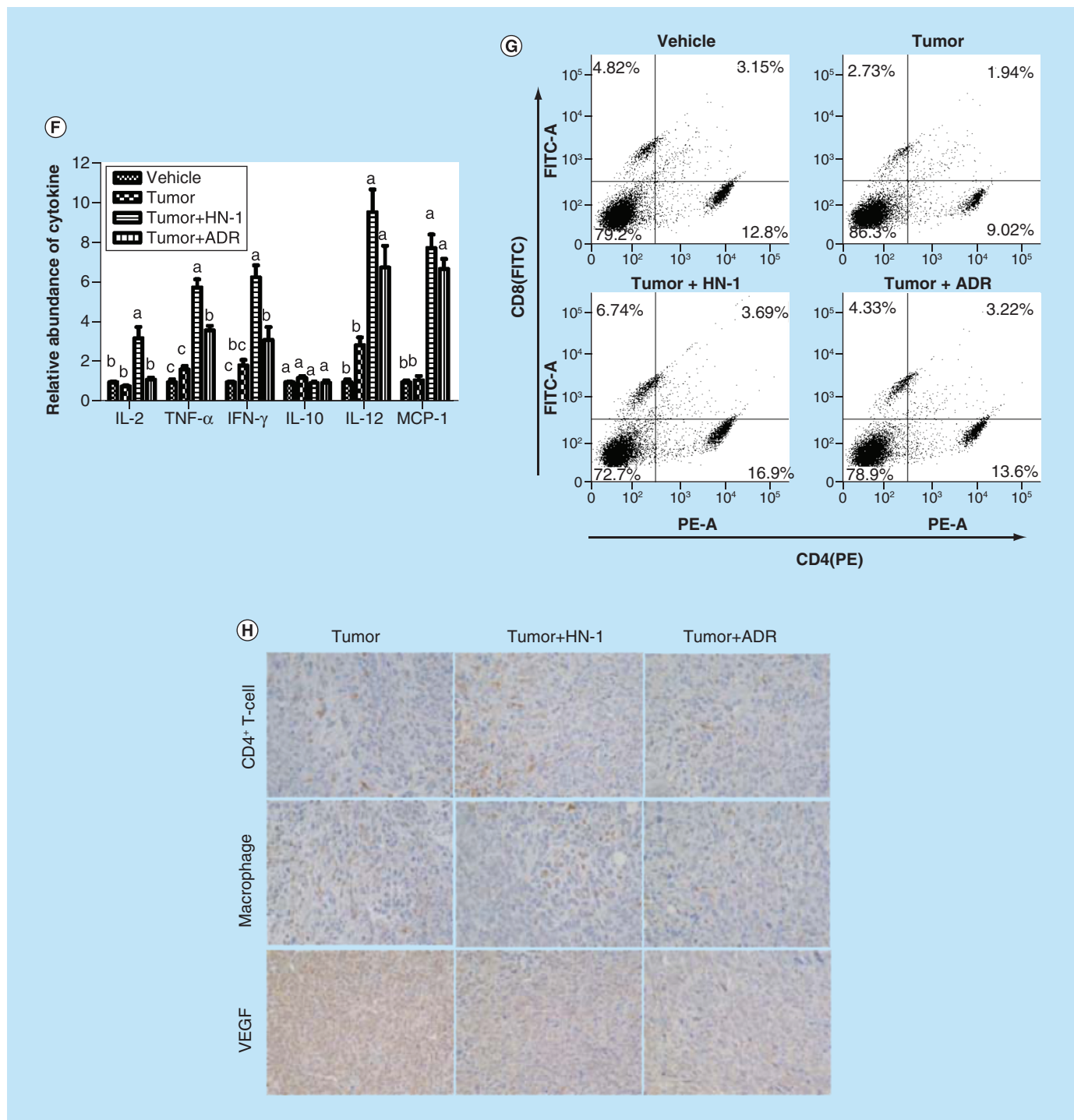


Figure 8. HN-1 inhibited tumor and activated antitumor immune response in a 4T1 murine breast cancer model without causing systemic toxicity (cont.). (A, B) HN-1 significantly inhibited the tumor growth in a 4T1 breast cancer models in BALB/c mice, and decreased tumors volume and weight (B). (C) HN-1 did not cause the weight loss of the mice during the treatment. (D) HN-1 dramatically lowered spleen index of tumor-bearing mice. (E) Hematoxylin & eosin staining was used to detect the histological changes of viscera after HN-1 and ADR treatment. (F) HN-1 remarkably increased the serum levels of cancer immunity-associated chemokines and cytokines in BALB/c-derived 4T1 mammary carcinoma model mice, including MCP-1, IL-2, TNF- α , IFN- γ and IL-12, but did not alter the IL-10 level statistically. (G) HN-1 significantly stimulated CD4⁺T-cell proliferation and increased the level of CD4⁺/CD8⁺ in spleen. (H) Immunohistochemistry revealed that HN-1 enhanced the infiltration of CD4⁺ T cells, and prevented the blood capillary formation, as evidenced by decreases of VEGF, but significantly decreased tumor-associated macrophages in solid tumor. Data are shown as mean ± standard error of the mean of three independent experiments.

*p < 0.05; **p < 0.01; ***p < 0.001 by Tukey's t-test. Letters on top of the bar charts indicate significant differences between control and experimental group by Duncan's multiple-range test. Tukey: compare pairs of columns.

ADR: Adriamycin; ns: Not significant.

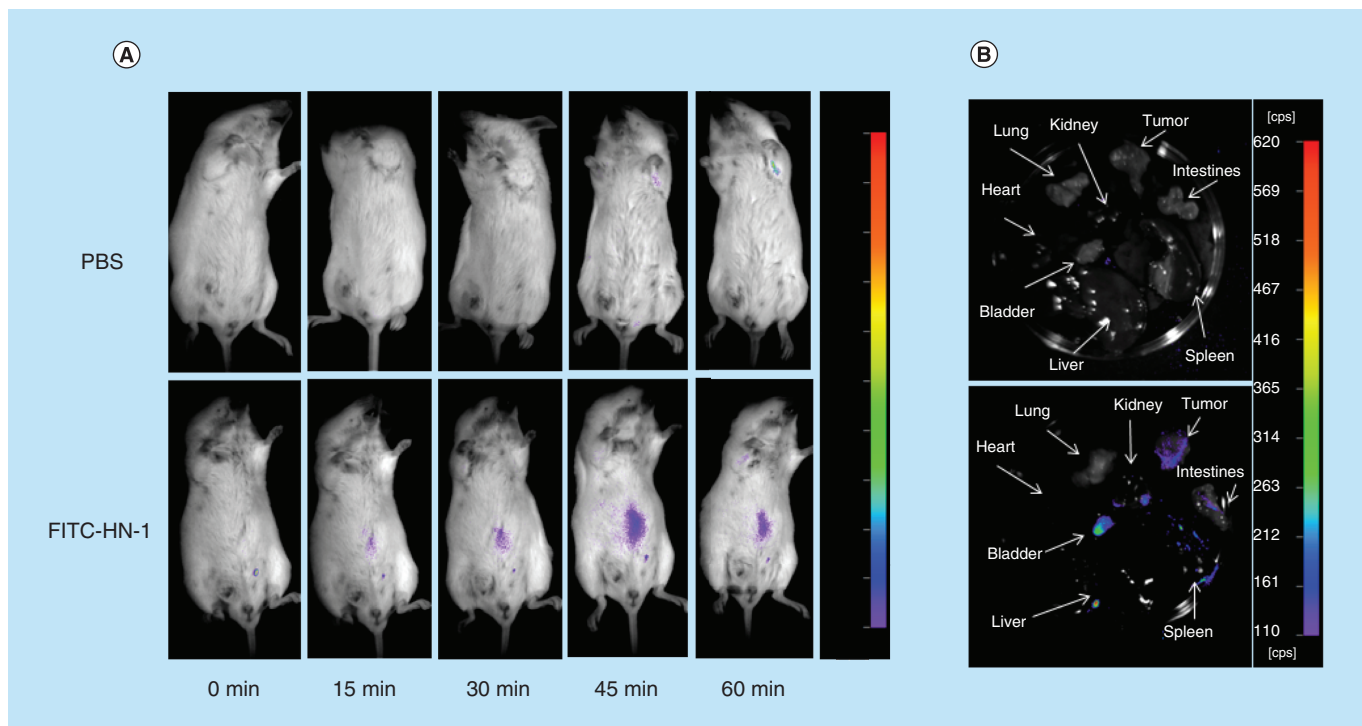


Figure 9. *In vivo* real-time imaging of HN-1 in tumor-bearing BALB/c mice. **(A)** Fluorescence imaging of 4T1 bearing mice after ip. injections of FITC-HN-1 at 0, 15, 30, 45 and 60 min. **(B)** Major organs were imaged for FITC-HN-1 fluorescence signal. ip.: Intraperitoneal.

drug dosages and the incidence/severity of side effects, but substantially reduces the likelihood of chemo- or radioresistance. However, co-delivery of immune-stimulatory and chemotherapeutic agents is badly hindered by the lack of effective management owing to their different drug profiles [22]. Where after, immune response elicited by chemotherapeutic agents is strikingly restricted by negative feedback during tumor development [20,21] and significant and cumulative systematic toxicities. These challenges have motivated us to evaluate the immune-based mechanisms of apoptogenic HN-1. Using BALB/c-derived 4T1 mammary carcinoma model that shares many similarities in immunogenicity, growth and metastasis with human mammary cancer [51], we show that HN-1 significantly stimulated CD4⁺ T-cell proliferation and increased the level of CD4⁺/CD8⁺, via regulating the levels of cancer immunity-associated cytokines/chemokines, such as IL-2, TNF- α , IFN- γ , IL-12 and MCP-1, resulting in marked tumor regression. Among them, IL-12 plays major roles in T-cell and B-cell activation in tumorigenesis, and enhance tumor-specific antibodies that destroy malignant cells [44], while MCP-1 mediates trafficking of monocytes/macrophages and stimulates TAMs cytotoxicity directly [46]. In concordance with the induction of IL-12, HN-1 induced CD8⁺ T-cells proliferation which are effector cells with high cytotoxicity against tumor cells. HN-1 also significantly increased IL-2 and IFN- γ production, which theoretically augment Th1 cellular immunity [42,44]. In the context of cancer, macrophages infiltrating solid tumors, usually called TAMs, share many hallmarks with alternatively activated (M2) macrophages, and promote cancer cell proliferation in virtue of their immunosuppressive and angiogenic effects, in support of tumor growth and metastasis [18]. Here, we observed a significant decrease of infiltrating TAMs in solid tumors and apparent reduction of blood capillaries in HN-1-treating tumor sections, indicating its capability to prevent metastases.

In addition to effective anti-tumor immunity, immunostimulatory agents also elicit serious toxicities, such as systemic cytokine storm and excessive vascular permeability, which are life-threatening and hamper their clinical application. Here, we showed that HN-1 *in vivo* induced no pathological toxicity and adverse effects of the main organs in mice, while ADR obviously destroyed heart structure, and failed to prevent the spleen swelling. As expected, HN-1 treatment alone did not stimulate the pro-inflammatory cytokine productions in mice macrophages, including MCP-1, MIP-2, IL-10 and TNF- α , IL-6, IL-1 β (Supplementary Figure 2), suggesting that HN-1 would not induce systemic cytokine release in response to the cancer immunotherapy. A number of peptide drugs developed

so far were ultimately discarded from clinical use due to poor stability, unsatisfactory tissue distribution followed by low bioavailability. Here, we analyzed the distribution pattern of HN-1 in mice as well as in selected organs *ex vivo*, revealing a good correlation between its biodistribution patterns with its on/off-target effects in the context of malignant solid tumor.

Altogether, our findings of both *in vitro* and *in vivo*, propose that HN-1 represents a novel immunochemotherapeutic agent in treating cancers especially chemoresistant ones that would supplement the use of immunotherapy or chemotherapy alone. As an antineoplastic agent, HN-1 induces caspase-independent cancer cells apoptosis through p53-dependent upregulation of Bax and downregulation of Bcl-2 via the modulation of MAPK (p38, JNK1/2 and ERK1/2)/NF-κB signaling pathway. More importantly, HN-1 stimulates both the innate and adaptive arms of the immune system and boosts cancer-resolving immunity without inducing potentially harmful pro-inflammatory responses, which severely hampers the clinical application of immunostimulatory agents. In particular, given the inhibitory efficacy of HN-1 in cancer metastasis and blood capillary formation, and safety as well as ideal distribution pattern, HN-1 could be employed in situations in which patients have a compromised immunity after major surgeries, or a high-dose myelosuppressive chemotherapy.

Future perspective

Discovery of a novel effective tumor-targeting peptide with immune regulating property is meaningful for cancer therapy, due to the urgent demand on novel immunochemotherapeutic agent. In addition, the obtained results may shed a new light to the design of rationale-based combined cancer treatments against cancer in the future.

Summary points

- A small host defense peptide, HN-1 significantly inhibited multiple malignant cells proliferation, even chemoresistant MCF-7/ADR (Adriamycin).
- HN-1 markedly inhibited tumor growth in a xenograft breast tumor model in nude mice.
- HN-1 induced the caspase-independent mitochondrial apoptosis, as indicated by a p53-dependent increase of Bax/Bcl-2 ratio and the nuclear translocation of AlF. It is the first time through our investigations, we show that host defense peptide could act through the caspase-independent pathway to mediate apoptosis in MCF-7 cells.
- HN-1 induced reactive oxygen species/MAPK and decreased NF-κB pathways to assist caspase-independent mitochondrial apoptosis.
- In addition to direct antineoplastic effect, HN-1 significantly stimulated T-cell proliferation and augmented CD4⁺/CD8⁺ in BALB/c-derived 4T1 mammary carcinoma model.
- HN-1 enhanced the serum levels of cancer immunity-associated effectors without inducing inflammation.
- HN-1 notably decreased the blood capillary formation and infiltration of the tumor-associated macrophages that supports the tumor growth and metastasis in tumor-bearing mice.
- More importantly, systemic administration of HN-1 in mice was well tolerated, and gave a good correlation between its biodistribution pattern with its on/off-target effects in tumor-bearing mice.

Supplementary data

To view the supplementary data that accompany this paper please visit the journal website at: www.futuremedicine.com/doi/full/10.2217/fmc-2019-0100

Financial & competing interests disclosure

This work was supported by the Chinese National Natural Science Foundation (31872223 and 31772455); Natural Science Foundation of Jiangsu Province (BK20160336 and BK20171214); Natural Science Foundation of College in Jiangsu Province (16KJB350004); Suzhou Science and Technology Development Project (SNG2017045); Qinglan Project of Jiangsu Education Department, the Priority Academic Program Development of the Jiangsu Higher Education Institutes (PAPD). The authors have no other relevant affiliations or financial involvement with any organization or entity with a financial interest in or financial conflict with the subject matter or materials discussed in the manuscript apart from those disclosed.

No writing assistance was utilized in the production of this manuscript.

Ethical conduct of research

The authors state that they have obtained appropriate institutional review board approval or have followed the principles outlined in the Declaration of Helsinki for all human or animal experimental investigations.

References

Papers of special note have been highlighted as: • of interest; •• of considerable interest

1. Von Hoff DD, Ervin T, Arena FP *et al.* Increased survival in pancreatic cancer with nab-paclitaxel plus gemcitabine. *N. Engl. J. Med.* 369(18), 1691–1703 (2013).
2. Malhotra V, Perry MC. Classical chemotherapy: mechanisms, toxicities and the therapeutic window. *Cancer Biol. Ther.* 2(4 Suppl. 1), S2–S4 (2003).
3. Thundimadathil J. Cancer treatment using peptides: current therapies and future prospects. *J. Amino Acids* 2012, 967347 (2012).
- 4. An overview on current therapies and future prospects of peptide drugs.
5. Mitchell EP. Gastrointestinal toxicity of chemotherapeutic agents. *Semin. Oncol.* 33(1), 106–120 (2006).
6. Goldman B. Multidrug resistance: can new drugs help chemotherapy score against cancer? *J. Natl Cancer Inst.* 95(4), 255–257 (2003).
7. Luqmani YA. Mechanisms of drug resistance in cancer chemotherapy. *Med. Prin. Pract.* 14(Suppl. 1), 35–48 (2005).
8. Kyi C, Postow MA. Checkpoint blocking antibodies in cancer immunotherapy. *FEBS Lett.* 588(2), 368–376 (2014).
9. Intlekofer AM, Thompson CB. At the bench: preclinical rationale for CTLA-4 and PD-1 blockade as cancer immunotherapy. *J. Leukocyte Biol.* 94(1), 25–39 (2013).
10. Callahan MK, Wolchok JD. At the bedside: CTLA-4- and PD-1-blocking antibodies in cancer immunotherapy. *J. Leukocyte Biol.* 94(1), 41–53 (2013).
11. Michallet M, Maloisel F, Delain M *et al.* Pegylated recombinant interferon alpha-2b vs recombinant interferon alpha-2b for the initial treatment of chronic-phase chronic myelogenous leukemia: a Phase III study. *Leukemia* 18(2), 309–315 (2004).
12. Pachella LA, Madsen LT, Dains JE. The toxicity and benefit of various dosing strategies for interleukin-2 in metastatic melanoma and renal cell carcinoma. *J. Adv. Pract. Oncol.* 6(3), 212–221 (2015).
13. Robert C, Thomas L, Bondarenko I *et al.* Ipilimumab plus dacarbazine for previously untreated metastatic melanoma. *N. Engl. J. Med.* 364(26), 2517–2526 (2011).
14. Prieto PA, Yang JC, Sherry RM *et al.* CTLA-4 blockade with ipilimumab: long-term follow-up of 177 patients with metastatic melanoma. *Clin. Cancer Res.* 18(7), 2039–2047 (2012).
15. Galluzzi L, Senovilla L, Zitvogel L, Kroemer G. The secret ally: immunostimulation by anticancer drugs. *Nat. Rev. Drug. Discov.* 11(3), 215–233 (2012).
16. Zitvogel L, Kepp O, Kroemer G. Immune parameters affecting the efficacy of chemotherapeutic regimens. *Nat. Rev. Clin. Oncol.* 8(3), 151–160 (2011).
17. Vincent J, Mignot G, Chalmin F *et al.* 5-Fluorouracil selectively kills tumor-associated myeloid-derived suppressor cells resulting in enhanced T cell-dependent antitumor immunity. *Cancer Res.* 70(8), 3052–3061 (2010).
- 18. Reveals that antitumor effect of 5FU is mediated, at least in part, by its selective cytotoxic action on MDSC.
19. Vanneman M, Dranoff G. Combining immunotherapy and targeted therapies in cancer treatment. *Nat. Rev. Cancer* 12(4), 237–251 (2012).
20. Bracci L, Schiavoni G, Sistigu A, Belardelli F. Immune-based mechanisms of cytotoxic chemotherapy: implications for the design of novel and rationale-based combined treatments against cancer. *Cell. Death Differ.* 21(1), 15–25 (2014).
21. Vacchelli E, Prada N, Kepp O, Galluzzi L. Current trends of anticancer immunochemotherapy. *Oncimmunology* 2(6), e25396 (2013).
22. Spranger S, Koblish HK, Horton B, Scherle PA, Newton R, Gajewski TF. Mechanism of tumor rejection with doublets of CTLA-4, PD-1/PD-L1, or IDO blockade involves restored IL-2 production and proliferation of CD8(+) T cells directly within the tumor microenvironment. *J. Immunother. Cancer* 2, 3 (2014).
23. Curran MA, Montalvo W, Yagita H, Allison JP. PD-1 and CTLA-4 combination blockade expands infiltrating T cells and reduces regulatory T and myeloid cells within B16 melanoma tumors. *Proc. Natl Acad. Sci. USA* 107(9), 4275–4280 (2010).
24. Chen Y, Xia R, Huang Y *et al.* An immunostimulatory dual-functional nanocarrier that improves cancer immunochemotherapy. *Nat. Commun.* 7, 13443 (2016).
- 25. Reports the development of a dual-functional, immunostimulatory nanomicellar carrier that is based on a prodrug conjugate of PEG with NLG919, an indoleamine 2,3-dioxygenase inhibitor currently used for reversing tumour immune suppression.
26. Hemshekhar M, Anaparti V, Mookherjee N. Functions of cationic host defense peptides in immunity. *Pharmaceutics* 9(3), 1–10 (2016).
- 27. Summarizes current literature on the wide range of functions of cationic host defense peptides in the context of the mammalian immune system.
28. Mansour SC, Pena OM, Hancock RE. Host defense peptides: front-line immunomodulators. *Trends Immunol.* 35(9), 443–450 (2014).
29. Ren SX, Cheng AS, To KF *et al.* Host immune defense peptide LL-37 activates caspase-independent apoptosis and suppresses colon cancer. *Cancer Res.* 72(24), 6512–6523 (2012).

- Reports human Cathelicidin LL-37 activates a GPCR-p53-Bax/Bcl-2 signaling cascade that triggers AIF/EndoG-mediated apoptosis in colon cancer cells.
26. Papo N, Shai Y. Host defense peptides as new weapons in cancer treatment. *Cell. Mol. Life. Sci.* 62(7–8), 784–790 (2005).
27. Furlong SJ, Mader JS, Hoskin DW. Bovine lactoferricin induces caspase-independent apoptosis in human B-lymphoma cells and extends the survival of immune-deficient mice bearing B-lymphoma xenografts. *Exp. Mol. Pathol.* 88(3), 371–375 (2010).
28. Hancock RE, Nijnik A, Philpott DJ. Modulating immunity as a therapy for bacterial infections. *Nat. Rev. Microbiol.* 10(4), 243–254 (2012).
29. Hancock RE, Sahl HG. Antimicrobial and host-defense peptides as new anti-infective therapeutic strategies. *Nat. Biotechnol.* 24(12), 1551–1557 (2006).
30. Roudi R, Syn NL, Roudbary M. Antimicrobial peptides as biologic and immunotherapeutic agents against cancer: a comprehensive overview. *Front. Immunol.* 8, 1320 (2017).
- An overview about the barriers to AMPs' clinical implementation and envision directions for further development.
31. Scott MG, Dullaghan E, Mookherjee N et al. An anti-infective peptide that selectively modulates the innate immune response. *Nat. Biotechnol.* 25(4), 465–472 (2007).
- Shows that an innate defense-regulator peptide was protective in mouse models of infection with important pathogens, especially the antibiotic-resistant bacteria.
32. Liu YY, Han TY, Giuliano AE, Hansen N, Cabot MC. Uncoupling ceramide glycosylation by transfection of glucosylceramide synthase antisense reverses adriamycin resistance. *J. Biol. Chem.* 275(10), 7138–7143 (2000).
33. Kurokawa M, Kornbluth S. Caspases and kinases in a death grip. *Cell* 138(5), 838–854 (2009).
34. Hu W, Ge Y, Ojcius DM et al. p53 signalling controls cell cycle arrest and caspase-independent apoptosis in macrophages infected with pathogenic Leptospira species. *Cell. Microbiol.* 15(10), 1642–1659 (2013).
35. Soengas MS, Lowe SW. Apoptosis and melanoma chemoresistance. *Oncogene* 22(20), 3138–3151 (2003).
36. Kook SH, Son YO, Chung SW et al. Caspase-independent death of human osteosarcoma cells by flavonoids is driven by p53-mediated mitochondrial stress and nuclear translocation of AIF and endonuclease G. *Apoptosis* 12(7), 1289–1298 (2007).
37. Zhang Y, Chen F. Reactive oxygen species (ROS), troublemakers between nuclear factor- κ B (NF- κ B) and c-Jun NH2-terminal kinase (JNK). *Cancer Res.* 64(6), 1902–1905 (2004).
38. Pearson G, Robinson F, Beers Gibson T et al. Mitogen-activated protein (MAP) kinase pathways: regulation and physiological functions. *Endocr. Rev.* 22(2), 153–183 (2001).
39. Al-Azayzih A, Gao F, Goc A, Somanath PR. TGFbeta1 induces apoptosis in invasive prostate cancer and bladder cancer cells via Akt-independent, p38 MAPK and JNK/SAPK-mediated activation of caspases. *Biochem. Biophys. Res. Commun.* 427(1), 165–170 (2012).
40. Park D-H, Xu HD, Shim J et al. Stephania delavayi Diels. inhibits breast carcinoma proliferation through the p38 MAPK/NF- κ B/COX-2 pathway. *Oncol. Rep.* 26(4), 833–841 (2011).
41. Heuvers ME, Aerts JG, Cornelissen R, Groen H, Hoogsteden HC, Hegmans JP. Patient-tailored modulation of the immune system may revolutionize future lung cancer treatment. *BMC Cancer* 12(1), 580 (2012).
42. Zhang Y, Li N, Suh H, Irvine DJ. Nanoparticle anchoring targets immune agonists to tumors enabling anti-cancer immunity without systemic toxicity. *Nat. Commun.* 9(1), 6 (2018).
- Demonstrates that anchoring IL-2 and anti-CD137 on the surface of liposomes allows these immune agonists to rapidly accumulate in tumors while lowering systemic exposure.
43. van Horssen R, Ten Hagen TL, Eggermont AM. TNF-alpha in cancer treatment: molecular insights, antitumor effects, and clinical utility. *Oncologist* 11(4), 397–408 (2006).
44. Ni J, Miller M, Stojanovic A, Garbi N, Cerwenka A. Sustained effector function of IL-12/15/18-preactivated NK cells against established tumors. *J. Exp. Med.* 209(13), 2351–2365 (2012).
45. Bellmann-Weiler R, Schroll A, Engl S et al. Neutrophil gelatinase-associated lipocalin and interleukin-10 regulate intramacrophage Chlamydia pneumoniae replication by modulating intracellular iron homeostasis. *Immunobiology* 218(7), 969–978 (2013).
46. Iida N, Nakamoto Y, Baba T et al. Tumor cell apoptosis induces tumor-specific immunity in a CC chemokine receptor 1- and 5-dependent manner in mice. *J. Leukoc. Biol.* 84(4), 1001–1010 (2008).
47. Vendramini-Costa DB, de Carvalho JE. Molecular link mechanisms between inflammation and cancer. *Curr. Pharm. Des.* 18(26), 3831–3852 (2012).
48. Lee HS, Park CB, Kim JM et al. Mechanism of anticancer activity of buforin IIb, a histone H2A-derived peptide. *Cancer Lett.* 271(1), 47–55 (2008).
49. Huang TC, Lee JF, Chen JY. Pardaxin, an antimicrobial peptide, triggers caspase-dependent and ROS-mediated apoptosis in HT-1080 cells. *Mar. drugs* 9(10), 1995–2009 (2011).

50. Park IJ, Kim MJ, Park OJ *et al.* Cryptotanshinone sensitizes DU145 prostate cancer cells to Fas(APO1/CD95)-mediated apoptosis through Bcl-2 and MAPK regulation. *Cancer Lett.* 298(1), 88–98 (2010).
51. Pulaski BA, Terman DS, Khan S, Muller E, Ostrand-Rosenberg S. Cooperativity of *Staphylococcal aureus* enterotoxin B superantigen, major histocompatibility complex class II, and CD80 for immunotherapy of advanced spontaneous metastases in a clinically relevant postoperative mouse breast cancer model. *Cancer Res.* 60(10), 2710–2715 (2000).

